Ozone profile retrieval from Global Ozone Monitoring Experiment (GOME) data using a neural network approach (Neural Network Ozone Retrieval System (NNORSY))

M. D. Müller and A. K. Kaifel
Center for Solar Energy and Hydrogen Research (ZSW), Stuttgart, Germany

M. Weber, S. Tellmann, and J. P. Burrows
Institute of Environmental Physics (IUP), University of Bremen, Bremen, Germany

D. Loyola
Remote Sensing Technology Institute (IMF), German Aerospace Center (DLR), Oberpfaffenhofen, Germany

Received 25 June 2002; revised 21 March 2003; accepted 14 April 2003; published 20 August 2003.

[1] The inverse radiative transfer equation to retrieve atmospheric ozone distribution from the UV-visible satellite spectrometer Global Ozone Monitoring Experiment (GOME) has been modeled by means of a feed forward neural network. This Neural Network Ozone Retrieval System (NNORSY) was trained exclusively on a data set of GOME radiances collocated with ozone measurements from ozonesondes, Halogen Occultation Experiment, Stratospheric Aerosol and Gas Experiment II, and Polar Ozone and Aerosol Measurement III. Network input consists of a combination of spectral, geolocation, and climatological information (time and latitude). In the stratosphere the method globally reduces standard deviation with respect to an ozone climatology by around 40%. Tropospheric ozone can also be retrieved in many cases with corresponding reduction of 10–30%. All GOME data from January 1996 to July 2001 were processed. In a number of case studies involving comparisons with ozonesondes from Hohenpeissenberg, Syowa, and results from the classical Full Retrieval Method, we found good agreement with our results. The neural network was found capable of implicitly correcting for instrument degradation, pixel cloudiness, and scan angle effects. Integrated profiles generally agree to within ±5% with the monthly Total Ozone Mapping Spectrometer version 7 total ozone field. However, some problems remain at high solar zenith angles and very low ozone values, where local deviations of 10–20% have been observed in some cases. In order to better characterize individual ozone profiles, two local error estimation methods are presented. Vertical resolution of the profiles was assessed empirically and seems to be of the order of 4–6 km. Since neural network retrieval is a mathematically simple, one-step procedure, NNORSY is about 10^3–10^5 times faster than classical retrieval techniques based upon optimal estimation. *INDEX TERMS:* 0340 Atmospheric Composition and Structure: Middle atmosphere—composition and chemistry; 0355 Atmospheric Composition and Structure: Thermosphere—composition and chemistry; 0394 Atmospheric Composition and Structure: Instruments and techniques; 1610 Global Change: Atmosphere (0315, 0325); 1640 Global Change: Remote sensing; *KEYWORDS:* ozone profile retrieval, Global Ozone Monitoring Experiment, nonlinear regression, neural computing, neural networks, ozone remote sensing

Citation: Müller, M. D., A. K. Kaifel, M. Weber, S. Tellmann, J. P. Burrows, and D. Loyola, Ozone profile retrieval from Global Ozone Monitoring Experiment (GOME) data using a neural network approach (Neural Network Ozone Retrieval System (NNORSY)), *J. Geophys. Res.*, *108*(D16), 4497, doi:10.1029/2002JD002784, 2003.

1. Introduction

[2] Although ozone contributes only about one millionth to the total mass of the atmosphere, it is one of the most active and important chemical constituents. Not only does it prevent harmful UV radiation from reaching the ground, but it strongly influences the stratospheric temperature distribution, and shares responsibility for summer smog, the oxidation capacity of the atmosphere and global warming. Determining the three-dimensional, global distribution of ozone from low Earth orbit has

0148-0227/03/2002JD002784$09.00

been a challenge to which a number of different satellite instruments have been assigned in the past. One of these is the Global Ozone Monitoring Experiment (GOME) [*Burrows et al.*, 1999] aboard the European polar orbiting satellite ERS-2. It is a scanning nadir viewing spectrometer that operates since 1995 and has for the first time the capability to measure ozone profiles down into the troposphere [*de Beek et al.*, 1997; *Hoogen et al.*, 1997; *Siddans et al.*, 1999; *van der A*, 1999]. GOME is a scaled down version of the Scanning Imaging Absorption spectrometer for Atmospheric Chartography (SCIAMACHY) instrument [*Burrows et al.*, 1995; *Bovensmann et al.*, 1999], which was recently launched aboard the Envisat satellite.

[3] In order to exploit this theoretical capability, a nonlinear, ill-posed inverse retrieval problem has to be solved for the Sun-normalized GOME radiances. To achieve this, various independent retrieval algorithms have been developed, most of which are based upon the principle of Optimal Estimation (OE) as described by *Rodgers* [1976, 1990]. Examples of these are the Full Retrieval Method (FURM) [*Hoogen et al.*, 1997, 1999], which relies on a specifically developed radiative transfer model GOMETRAN [*Rozanov et al.*, 1997] as the forward model. The same forward model is also being used in another retrieval scheme [*Siddans et al.*, 1999], where a two-step OE algorithm first retrieves a stratospheric first guess profile from short wavelengths, then the final profile using the longer wavelengths. *Hasekamp et al.* [1999] have compared OE with a Philips-Tikhonov regularization scheme and have found similar performance. There is also an operational near real-time ozone profile retrieval system [*van der A et al.*, 2001], which is also based on OE, but uses the LIDORT forward model [*van Oss and Spurr*, 2001].

[4] All these retrieval schemes can be considered geophysical, since they rely on the relatively well understood forward calculation of the radiative transfer equation. Yet they also possess a significant statistical component, the reliance on a priori information in the form of an ozone climatology. In addition, they require certain assumptions about unmeasurable or unavailable parameters of the state of the atmosphere and about the instrument behavior. This paper proposes to combine these building blocks in a different way, by using geophysical knowledge and some assumptions to find a suitable structure for a primarily statistical method, which takes care of other unknown parameters on its own. This has been done successfully in other fields of atmospheric science [*Krasnopolsky*, 1997; *Chevallier et al.*, 1998; *Jiménez*, 2000; *Aires et al.*, 2001] with the statistical tool of choice being a nonlinear feed forward neural network. The motivation behind the development of the Neural Network Ozone Retrieval System for GOME Data (NNORSY-GOME) is that it complements existing retrieval algorithms and is faster by several orders of magnitude.

[5] Section 2 of this paper gives a brief theoretical introduction. In section 3 we describe the specific data and methods needed to retrieve ozone profiles from GOME. The results are presented in section 4 along with an error analysis. Since the latter poses a number of neural network specific difficulties, we devote section 5 to examine and evaluate our method in several case studies. Section 6 will conclude the paper.

2. Theory

[6] The idea of retrieving height-resolved ozone information with an orbital instrument measuring backscattered UV (BUV) radiation dates back to the 1950s [*Singer and Wentworth*, 1957]. Ozone is particularly suited for this task, because its absorption coefficient rises steeply by about four orders of magnitude when moving from $\lambda = 340$ nm to 260 nm in the so-called Hartley continuum. This alone for solar radiation would already lead to decreasing penetration depth in the atmosphere, but the effect is greatly enhanced by Rayleigh scattering, which increases with λ^{-4}, and by the exponentially increasing air pressure, i.e., scatterer density. As a result, incoming radiation observes an almost transparent atmosphere down to a certain depth, at which extinction rises rapidly within a few kilometers. The height of this layer depends on wavelength; it almost acts like a fuzzy mirror, with the reflected photons carrying ozone information mostly from the particular height region. By scanning the UV, one can thus obtain a height-resolved ozone profile. However, only a small fraction of the UV radiation reflects from below the ozone peak, and it has been shown that tropospheric ozone retrieval is very difficult and severely stresses the detection limits of the GOME instrument [*de Beek*, 1998].

[7] This paper proposes a fully connected feed forward neural network, also called multilayer perceptron [*Rumelhart et al.*, 1986], to perform the inversion of GOME spectra. Here, we will only give a brief summary of the theory (refer to Appendix A for more details). Essentially, we assume that a mapping between spectral data and ozone exists, which can be approximated by the neural network model $\mathbf{R}$ according to

$$\mathbf{x} = \mathbf{R}(\mathbf{y}, \mathbf{c}, \mathbf{w}) + \boldsymbol{\epsilon}, \tag{1}$$

where $\mathbf{x}$ is the ozone profile, $\mathbf{y}$ the spectral GOME data, $\mathbf{c}$ a vector of supplementary input parameters, $\boldsymbol{\epsilon}$ an error vector, and $\mathbf{w}$ contains the network model parameters, also called weights. When certain preconditions are observed, it has been proven that the neural network can theoretically approximate any given mapping with arbitrary accuracy [*Hornik et al.*, 1989]. In contrast to conventional approximation schemes with fixed basis functions (e.g., polynoms, trigonometric functions, etc.), where the approximation error increases exponentially with the dimension of the mapping, the errors from approximation tasks carried out by means of neural networks were shown to be independent of the mapping dimension [*Baron*, 1994].

[8] To find an optimal set of weights $\hat{\mathbf{w}}$, a training data set of T paired spectral and ozone profile measurements, $\{(\mathbf{y}^p,\mathbf{c}^p), \mathbf{x}^p\}$, $p = 1,\ldots,T$, is employed. This data set is used in a learning algorithm (see section 3.4) to perform a nonlinear optimization with respect to $\mathbf{w}$ to find the minimum of the error function

$$E = \frac{1}{2}\sum_{p=1}^{T} (\mathbf{R}(\mathbf{y}^p, \mathbf{c}^p, \mathbf{w}) - \mathbf{x}^p)^2. \tag{2}$$

[9] Once this is done, the resulting mapping $\hat{\mathbf{R}}$ is optimal in a global sense, and can be applied to all observations solely as a forward model. This is in contrast to the OE method, which determines a new, locally optimal solution from each individual observation.

3. Data and Methods

[10] The NNORSY method relies on collocations of GOME pixels with measured ozone profiles from different sources to form the training and test databases. The maximum distance for collocations was set to 250 km, with no more than 12 h between independent ozone and GOME measurements. All data selected were interpolated to a common height grid and converted to average ozone number densities at 1, 2, . . ., 60 km geopotential height.

3.1. Ozone Profile Collocations

[11] Ozonesonde data were obtained from the World Ozone and Ultraviolet Radiation Data Center (WOUDC) [*Wardle et al.*, 1998] and from the Southern Hemisphere Additional Ozonesondes (SHADOZ) campaign [*Thompson et al.*, 2003]. These data generally have a high-quality and high vertical resolution, but their geographical distribution is uneven, with most stations located at northern midlatitudes and very few measurements over the oceans. Since sonde data starts becoming unreliable around 25–30 km [*Stratospheric Processes and Their Role in Climate* (*SPARC*), 1998], all sonde profiles were cut off at a random altitude within this range. Cutting off all sondes at the same height resulted in artifacts in the retrieved profiles and was therefore avoided. To obtain coverage of higher altitudes, sonde data were supplemented by satellite data from solar occultation limb sounders. These included Halogen Occultation Experiment (HALOE) [*Russell et al.*, 1993] data version 18 [*Lu et al.*, 1997], Stratospheric Aerosol and Gas Experiment (SAGE) II [*Cunnold et al.*, 1989] data version V6.10 [*Cunnold et al.*, 2000], and Polar Ozone and Aerosol Measurement (POAM) III Version 3 data [*Lucke et al.*, 1999; *Lumpe et al.*, 2002]. HALOE and SAGE II sample the entire globe quite evenly between 70°S and 70°N, while the POAM geometry results in sunrise events occurring between 54°N and 71°N, and sunset events between 63°S and 88°S.

[12] As has been found elsewhere [*Lu et al.*, 1997; *Steele and Turco*, 1997; *Deniel et al.*, 1997; *SPARC*, 1998], the aforementioned ozone data sources do not always agree. The neural network will construct a compromise between the different sources, therefore biases stemming from different measurement principles and retrieval algorithms for the limb sounders are likely to cancel out. Yet it is clear that strong biases and variances in the training data set will adversely affect NNORSY retrieval accuracy, therefore some homogenization based on the statistical properties of the training data set was performed. Since both the distribution of collocations and of ozone in general are largely governed by latitude, the statistics of latitude bands were used for this purpose.

[13] First, the number of collocations as a function of latitude and time had to be checked. An over representation of certain latitude regions might lead to biases in the neural network output, since it favors certain types of profiles [*Bishop*, 1995]. On the other hand, it is reasonable to include more profiles from latitudes where natural ozone variability is higher, for example, near the edge of the polar vortex and at winter/spring northern midlatitudes, such that a greater number of different atmospheric conditions is sampled (Figure 1a). Profiles are removed by selectively reducing the allowed maximum collocation distance. The availability of data over the years has to be controlled in a similar manner (Figure 1b), otherwise modeling of ozone trends and correction of sensor degradation effects could introduce a bias.

[14] It is clearly seen in Figure 1a, that the highest density of collocations is located around 50°–60°N. POAM data in the NH have therefore been used only poleward of 65°N, to extend data coverage toward the pole, because SAGE and HALOE measurements become sparse in this region. The withheld POAM data from 54°–65°N can later be used for validation purposes.

[15] In a second step, the remaining collocations are checked for consistency within 20° latitude bands, and heuristics were developed for sorting out suspicious ozone measurements. Details on this procedure can be found in [*Müller*, 2002].

3.2. GOME Level 1 Data

[16] The GOME data used for profile retrieval were processed with the standard GOME Data Processor Extraction program (Version 2.0), including all standard corrections (straylight, polarization, etc.) except spectral degradation due to UV radiation exposure, which the program applies equally to solar and Earth spectra. Thus it cancels out when calculating Sun-normalized radiances. Different degradation rate for solar and earthshine spectra after 1999 is not corrected but is automatically compensated for by the network. Also, no problems with wavelength shifts of the input data were observed.

[17] Retrievals were performed using the maximum horizontal resolution of the ground pixel of 320 km × 40 km. This required assigning the GOME Channel 1a spectra (ground coverage of 960 km × 100 km) to each of the smaller eight pixels covered by Channel 1b and 2 spectra. Channel 1a spectra are integrated 12 s instead of 1.5 s to increase the S/N ratio. Backscan pixels do not contribute notably to the horizontal resolution and were thus omitted. Apart from that, all GOME pixels regardless of cloudiness and ground condition were retained.

3.3. Other Data

[18] There is a considerable correlation between the ozone profile and the atmospheric temperature profile due to the fact that ozone controls part of the temperature variations by absorption of UV radiation. Temperature profiles from the UK Met Office (UKMO) [*Swinbank and O'Neill*, 1994] were therefore included into the neural network input. These data are available as global analysis fields every 24 hours at a horizontal resolution of 3.75° lon. × 2.5° lat., and were interpolated to the GOME pixel locations.

3.4. Neural Network Configuration

[19] The neural network used for the retrievals has 122 input, 45 hidden, and 60 output neurons. Table 1 shows the configuration of the neural network input layer. GOME

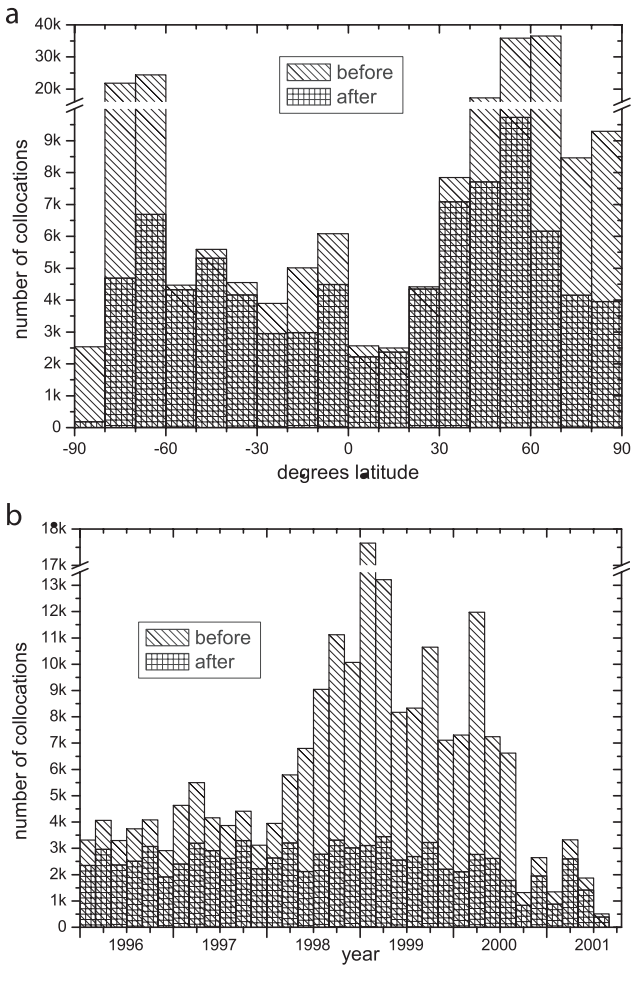

Figure 1. Training data distribution by (a) latitude and (b) time, before and after the data set homogenization procedure was applied.

Sun-normalized radiance values are mainly taken from the ozone Hartley and Huggins bands, where most of the ozone information resides. Additional spectral windows provide information on cloud cover and ground albedo. The spectral resolution has been degraded without significantly losing small-scale structure in the ozone absorption, by coadding of 4–12 wavelengths (0.35–1.5 nm). This reduces random noise and the number of free parameters (weights) in the network. The choice of spectral data presented in Table 1 yielded the best results in a series of systematic experiments. It should be noted that because of the flexibility of neural networks, the method is not very sensitive toward the selection and resolution of wavelength windows, as long as they contain enough physical information altogether. For instance, a completely different input setup with very broad coadding (1–10 nm resolution) below 290 nm, more values in the Chappuis bands and no data above 675 nm [*de Beek*, 1998] did not yield significant differences to the standard network.

[20] As discussed in section 2, apart from the spectral measurements a number of geophysical parameters are provided to the network. These include solar and satellite zenith angles and the scan angle, as well as three separate flags to account for the pixel type (east, nadir, west). Latitude and season allow the implicit construction of some sort of climatology, while the continuous in-orbit time provides a means to correct time-dependent degradation effects to a certain extent. The UKMO temperature profile was provided because of its strong correlation to atmospheric ozone.

[21] The neural network has been trained using Resilient Propagation (RPROP) [*Riedmiller and Braun*, 1993], which is related to the commonly employed error backpropagation algorithm [*Rumelhart et al.*, 1986]. In previous ozone retrieval applications [*Kaifel and Müller*, 1999; *Müller et al.*, 2001], it has been shown that RPROP is well suited for this kind and volume of data.

4. Results and Discussion

4.1. Global Test Data Set Validation

[22] The standard method for evaluating the quality of neural network output is to assess the error statistics on a test collocation data set independent of the training data. Care has been taken to prevent any ozone profiles from appearing in both training and test data, which can happen when multiple GOME pixels lie within the collocation radius. Also, collocations with ozonsondes from Hohenpeissenberg (WMO 99) and Syowa (WMO 101) were explicitly removed from both training and test data set. The test data set constructed consists of 12281 collocations with a distribution similar to the training data (70048 colloc.).

[23] Figure 2 shows the global error statistics of network output **o** compared to both training and test collocations **t**. With $d_p = o_p - t_p$, note that relative standard deviation is defined for each altitude level as

$$\text{rel.}\quad \sigma = \frac{\sum_p^T \sqrt{[1/(T-1)](d_p - \bar{d})^2}}{\frac{1}{T}\sum_p^T t_p}, \tag{3}$$

not as $\sqrt{\frac{1}{T-1}\sum(d_p - \bar{d})^2/t_p}$. Since we do not use averaging kernels or other smoothing methods, sonde profiles used in the collocations were only integrated to 1 km layers. Retrieval vertical resolution is probably considerably lower (see section 4.4). This would give rise to extreme relative errors due to unresolved fine structure whenever the latter calculation method is applied.

Table 1. Neural Network Input Parameters for Ozone Profile Retrievals[a]

Input Parameter	Number of Neurons	Purpose
270-325 nm	74	O_3 Hartley/Huggins band
380-385 nm	13	atmospheric window
598-603 nm	6	O_3 Chappuis band
758-772 nm	9	O_2 A-band: cloud detection
Satellite and solar zenith angles	4	slant column correction
line-of-sight flags	3	slant column correction
Latitude and season	2	ozone climatology background
In-orbit time	1	instrument degradation corr.
UKMO T-profile	10	atmospheric state info

[a]The wavelength ranges refer to Sun-normalized and logarithmized radiances measured by the GOME instrument.

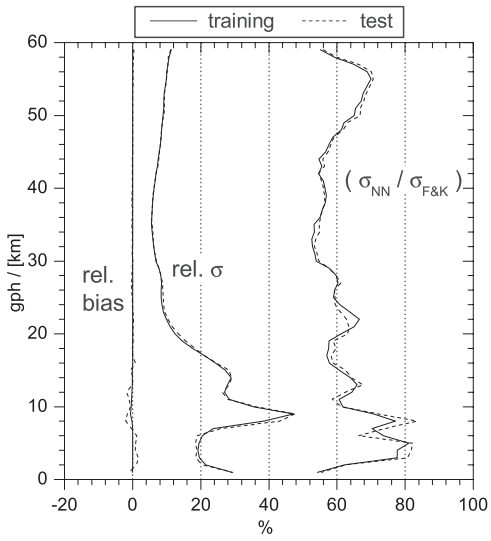

Figure 2. Global relative statistics of NNORSY ozone profile retrievals compared to training and test data set collocations. σ denotes standard deviation, whereby σ_{FK} is calculated by using profiles from the *Fortuin and Kelder* [1998] climatology instead of retrievals.

[24] As can be seen in Figure 2, there is a negligible bias between the collocations and NNORSY output. This is a property of the quadratic neural network error function [*Bishop*, 1995], and shows the importance of constructing a representative training data set. Overall, NNORSY-GOME reduces the standard deviation of the monthly mean *Fortuin and Kelder* [1998] (hereinafter referred to as FK) climatology with respect to the collocated sonde and limb sounder data by around 20–45%, depending on height. Similar results were obtained when comparing the reference network with a network trained using only climatological predictors as input (i.e., latitude and time, no spectral data).

[25] Test data set errors are only marginally higher than the ones from the training data, which is a sign of the good generalization ability of the network. Some other features which can be recognized in the figure are the sharp peak in the relative error around 9 km geopotential height (gph). Since the retrievals still reduce standard deviation wrt. the climatology, it can be concluded that this peak is mostly due to the high temporal and spatial variability of ozone in this layer, which are not well represented in monthly zonal means. The errors in the lower troposphere are also surprisingly low, considering the fact that gaining ozone information from GOME data in this height range is severely limited by clouds [*Hoogen et al.*, 1999]. However, there seem to be strong correlations between ozone values retrieved in the troposphere as discussed later in section 4.4.

[26] Sensitivity studies were performed by dividing the test data set into subsets according to input parameter values. Of these, the latitudinal dependency of the errors will be discussed below. No significant dependency on pixel line of sight was detected. With time, the errors do not follow a significant trend, although in the stratosphere errors for 2001 tend to be higher than usual. This can be explained in part by the underrepresentation of training data from 2001. It will be further investigated in a case study (section 5.5).

4.2. Latitudinal Statistics

[27] Figure 3 displays the relative statistics for the test data set divided into zonal bands 30° wide. The error characteristics of this approach vary considerably with latitude. This results from a combination of the latitudinally uneven distribution of training data (especially of ozonesondes) and the meridional dependence of ozone variability. For instance, in the SH polar region 1245 out of 1704 collocations stem from limb sounders, which obviously contribute considerable information the stratosphere, but sonde data are rare; therefore the tropospheric standard deviation is fairly high. The generally large solar zenith angles (SZAs) in this region also contribute to this problem. In the north polar region there are ample ozonesonde data (49%) available, but satellite data are missing north of 71°N. Thus the network has enough data to learn a suitable SZA correction for the lower heights, but the relatively low errors above 20 km are somewhat misleading, since they can only be computed from satellite profiles southward of

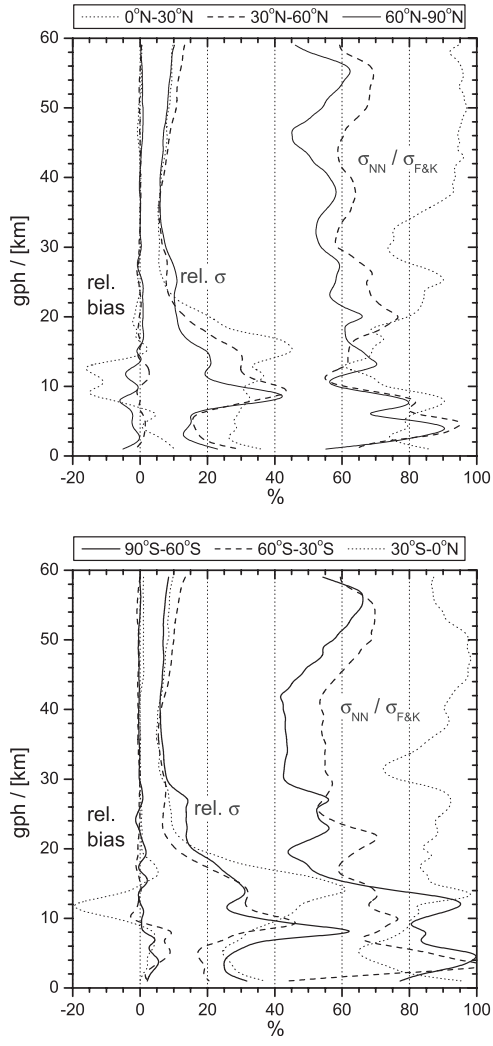

Figure 3. Same as Figure 2, but only test data set, divided into different latitude strips.

71°N, therefore errors closer to the pole might be somewhat higher as discussed later in section 5.5.

[28] In the tropics, the climatology obviously reproduces the ozone concentration above 20 km rather well, with NNORSY yielding a less significant reduction in standard deviation. This is due to the low ozone variability in this part of the atmosphere, where ozone distribution is mostly governed by photolytic ozone production, not by short-term transport and chemical processes. We also note a low bias of up to 20% in the region around 12 km, the reason of which is not completely understood. A combination of different effects are suspected to contribute, like frequent cloud occurrence, fewer number of collocations, and model errors resulting from the distinctively non-Gaussian error distribution at these heights (see Appendix A). However, because of the low ozone concentration in the tropical troposphere, in absolute terms this bias amounts to only $\sim 0.1 \cdot 10^{18}\ \mathrm{m}^{-3}$, and is thus easily offset globally, with the average extratropical ozone concentration at 12 km ranging around $2 \cdot 10^{18}\ \mathrm{m}^{-3}$.

4.3. Profile Error Estimation

[29] The test data set statistics presented in the previous sections may in principle be used as a crude accuracy estimate for the ozone profiles. They encompass GOME spectral measurement noise, collocation errors and biases between the different collocated profiles. Not included are errors due to the spatial and temporal distribution of training data, i.e., errors connected to the representativeness of the training collocations. These come into play especially in places where collocations are sparse, at the north pole for instance, and over the SH oceanic troposphere. Also not included is the deviation of sonde and limb sounder profiles from the true ozone distribution, i.e., the accuracy of the collocated profiles.

[30] On the other hand, a precision estimate for individual retrieved profiles would be desirable for a number of applications. Simply assigning noise estimates to the input data and adding quadratic errors of all input data modified with the neural network Jacobian did not result in useful error estimates, the errors are unrealistically high, contradicting experience made with the case studies in the following sections. A reason for this may be related to input error correlations, which the neural network compensates to a certain degree, leading to an effectively less-than-quadratic error summation. Error estimation methods have been extensively investigated in current literature [e.g., *Papadopoulos et al.*, 2001, and references therein], but most applications deal with fairly small data sets, for which an enhanced network can be constructed to approximate parameters of the output probability density [*Bishop*, 1995], or multiple networks can be trained and their spread interpreted statistically [*Lawrence et al.*, 1997]. While the latter method is being considered in future operational regime, it is too costly to implement as long as the system hasn't reached a stable state. The former method commonly involves massive increases in the number of output neurons, which would unbalance network and training data set size.

[31] Thus two other alternatives have been investigated. One of them is a brute force approach, in which the retrieval is repeated many ($\sim 10^3$) times while the input data is perturbed using realistic assumptions about measurement noise distributions. This method is feasible because of the high retrieval speed, and results in a precision estimate without the need for linear approximations.

[32] The second method investigated has been inspired by C. Satchwell (1994) (verbal presentation, cited by *Bishop* [1995]). We trained a second neural network with exactly the same structure and input data as the retrieval network, but replaced the training collocations with the absolute difference between the retrievals and the collocated O_3 profiles. The second network learns the dependence of error magnitude on the input data, giving an error estimate similar to the one provided in the previous two sections, but this time for individual profiles. This can be viewed as the profile accuracy. Because of the neural network property of reproducing the conditional average of the output, these error estimates when applied to the entire training data set sum up to give the same picture as presented in section 4.1.

[33] Overall, the errors calculated this way vary reasonably with the input data, reaching higher values in conditions and height ranges where low ozone concentrations coincide with high ozone variability, mostly within the Antarctic ozone hole (1σ-error: 50–80%), around the tropical upper troposphere (30–50%) and the midlatitude tropopause (20–30%). In other cases errors are about 5–20%. The brute force precision error exhibits quite a similar height dependency, but is generally lower by a factor of 1.5 to 2, as was expected since it encompasses fewer error sources.

4.4. Vertical Resolution

[34] The estimation of vertical resolution via averaging kernels (AKs) [*Rodgers*, 1990], as commonly used for classical retrieval schemes like OE, is not suitable for the neural network system presented here. This is due to its highly nonlinear modeling of input covariances [*Aires et al.*, 2001], its global nature and the intrinsic mixing of physical and statistical information.

[35] From visual impression, it is clear that the NNORSY profiles are oversampled, i.e., effective resolution is worse than the 1 km output grid. Ozonesondes and the occultation instruments used for collocation thus have a better resolution than NNORSY in almost all cases. A considerable part of the differences between retrievals and collocations in Figure 2 can therefore be attributed to smoothing [cf. *Rodgers*, 2000]. By artificially degrading the collocations' height resolution until smoothing errors on the collocation data sets were minimal, we have found that our retrievals have a vertical resolution of around 3–5 km in the 15–32 km geopotential height range, where the estimate is most reliable. The fact that this estimate is lower than the theoretical limit of 6–8 km commonly stated for OE based retrievals [*Hoogen et al.*, 1999; *van der A et al.*, 2001] may be surprising at first, but is confirmed by visual comparison (e.g., Figure 4 below). This effect arises from the more direct use of statistical information by the network; that is, it does not have to rely on a monthly mean a priori ozone profile, but can use the latitude and time predictors to internally generate a more detailed climatological representation of the ozone field, which better reflects variable features like, for instance, the ozone hole.

[36] An independent resolution estimate was gained from observing the retrieval error covariances exhibited by the

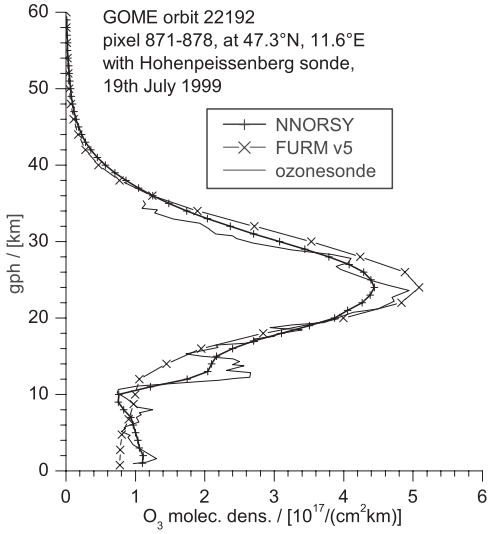

Figure 4. Example profile comparison with FURM retrieval and ozonesonde.

brute force error estimation method described in section 4.3. The error correlation lengths found here are in good correspondence with the above resolution estimate. Above 30 km gph the correlation length rises continuously, to reach values of around 11 km at the top of the profile. This reflects the smoothness of the occultation sounder profiles used to train the network, not a limitation of the method itself: If a sufficient number of high-resolution upper stratosphere ozone profiles were used for training, there is no reason why the network should not be able to extract the corresponding ozone information from the spectral input data, as it apparently does in the lower height ranges.

[37] Both methods fail to give accurate vertical resolution estimates in the troposphere because of long-range correlations with the profile above the ozone peak, interference from the lower stratosphere, and a lot of case-by-case variation. As a rough estimate, we seem to be getting between one and three independent ozone density values below 15 km gph.

5. Case Studies

5.1. Other Retrieval Algorithms

[38] Figure 4 shows two profiles retrieved by NNORSY and the Full Retrieval Method (FURM), an optimal estimation based retrieval scheme [*Hoogen et al.*, 1997]. The retrievals are averaged from up to eight GOME pixels for FURM, and up to six (skipping the backscan pixels) for NNORSY, however FURM averages the spectra whereas NNORSY averages the retrieved profiles. Also, a collocated ozonesonde measurements from Hohenpeissenberg is plotted. It can be observed that while both methods capture the maximum of the ozone density and the general structure of the profile, only NNORSY gives a hint at the secondary ozone maximum at around 13 km present in the high-resolution sonde profile. The tropospheric ozone distribution is also detected fairly well with NNORSY, although fine structure is not resolved. Both GOME retrieval methods seem to be systematically high above the primary ozone maximum, but this may also be a specific problem at altitudes above 27–30 km with Brewer-Mast ozonesondes used regularly in Hohenpeissenberg [*Kerr et al.*, 1994].

5.2. Hohenpeissenberg Ozonesondes

[39] Figure 5 depicts the timeline of both NNORSY retrievals and Hohenpeissenberg ozone sonde data. For this comparison, layers of 10 km GPH thickness have been calculated to reduce errors resulting from the different vertical resolution of the ozone profiles.

[40] The timeline plots show good agreement between NNORSY and the sondes in all height ranges, in particular, between 10 and 20 km. Note that for these plots, all GOME collocations found within 250 km of a given ozonesonde launch were averaged into a single profile. As expected, largest deviations arise in spring, where temporal and spatial ozone variability at northern midlatitudes is high. There is, however, no significant bias or drift of the NNORSY partial columns with respect to the sondes, even after beginning of the year 2001, when the ERS-2 satellite was switched to gyroless mode and the operational GOME Level 1 data started developing a number of problems. Apart from this, it is obvious that the neural network is sophisticated enough to implement a correction for radiance data degradation effects based on the input data. The FK climatology, also shown in the figure, cannot reproduce the short term changes in the ozone columns, and seems to be biased to higher values in the 20 to 30 km height range, which might hint at noticeable ozone losses in this height range [*Reid et al.*, 2000], since the climatology is compiled from data in the time frame 1980–1991.

[41] Figure 6 shows the same data set, this time averaged over 5 km layers and plotted as scatter graphs. The highest (Pearson) correlation coefficients of 0.90 and 0.94 are observed in the height range 10 to 20 km confirming the visual impression from Figure 5. In the 5 to 10 km range, NNORSY reproduces the low-ozone tropospheric background fairly accurately, but the points spread out for higher ozone values, such as those induced by stratosphere-troposphere exchange processes and tropospheric photochemistry [*Lelieveld and Dentener*, 2000]. Ozone retrieval is severely hampered by clouds in these cases, and collocation errors are high because of the events' short timescale and range. However, the linear regression curve is almost diagonal, and NNORSY outperforms the climatology considerably in that it generally seems to detect high-ozone laminae, even if the magnitude is not always correctly retrieved. The first two plots also show that obviously, at least two independent tropospheric ozone layers can be retrieved here (see section 4.4) The scatterplots for the lowest and the two uppermost layers do not exhibit any special features. Note once again the high bias of the FK climatology above 20 km.

5.3. Syowa Ozonesondes

[42] A slightly different picture is obtained when looking at similar plots from the Japanese Syowa station on the Antarctic continent (Figure 7). This station was also not used in training the network. The scatter of values in the tropospheric layers is more pronounced than at Hohenpeissenberg, making predictions of the network questionable below 10 km. Since these GOME measurements are typically taken at high solar zenith angles, weighting functions for tropospheric ozone may well be shifted toward longer

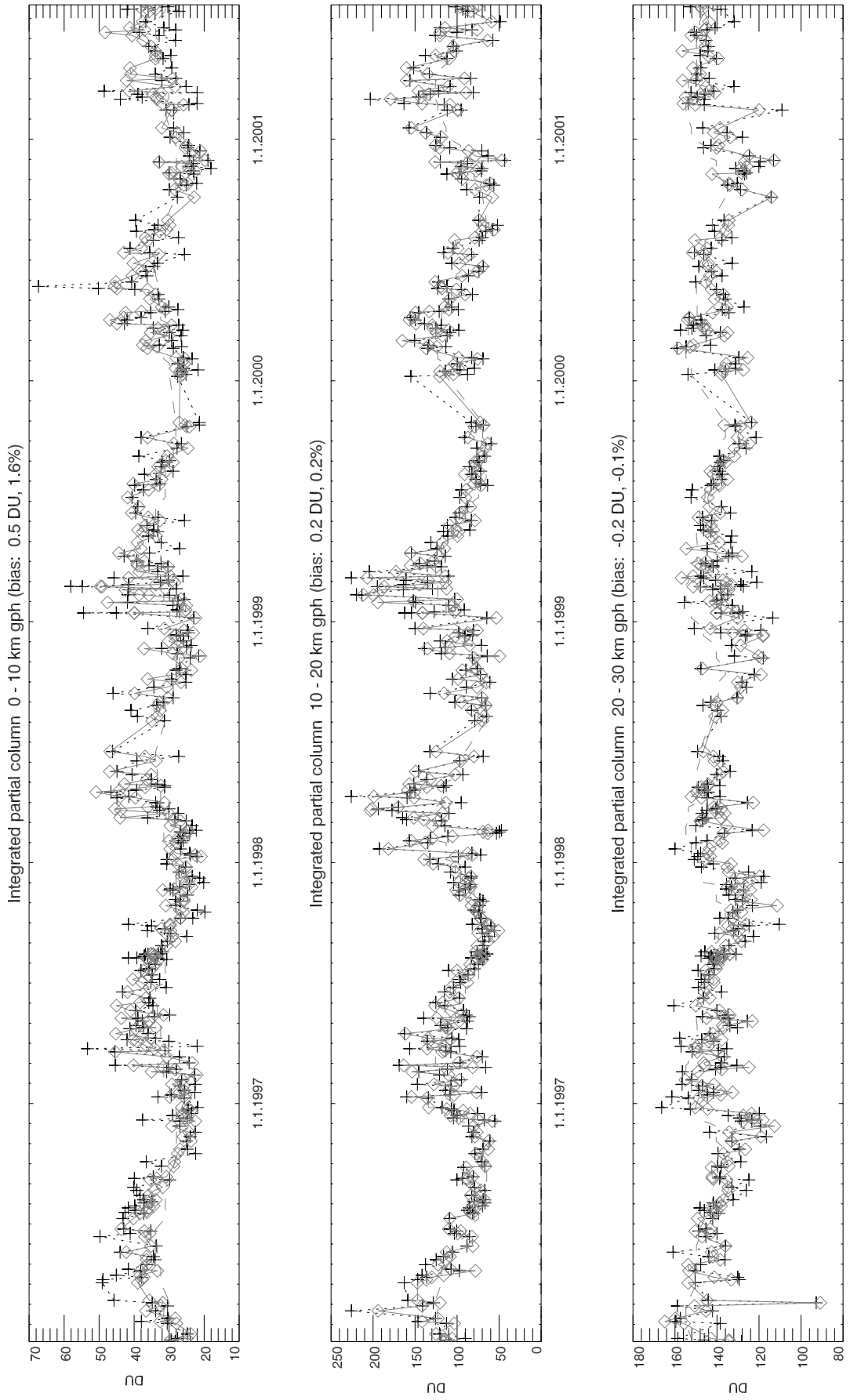

Figure 5. Timeline of partial ozone columns from NNORSY (diamonds) and collocated Hohenpeissenberg (47.8°N, 11.0°E) ozone sondes (pluses). Multiple collocations within 160 km were averaged into single points. The FK climatology is plotted for comparison as a dashed curve. See color version of this figure at back of this issue.

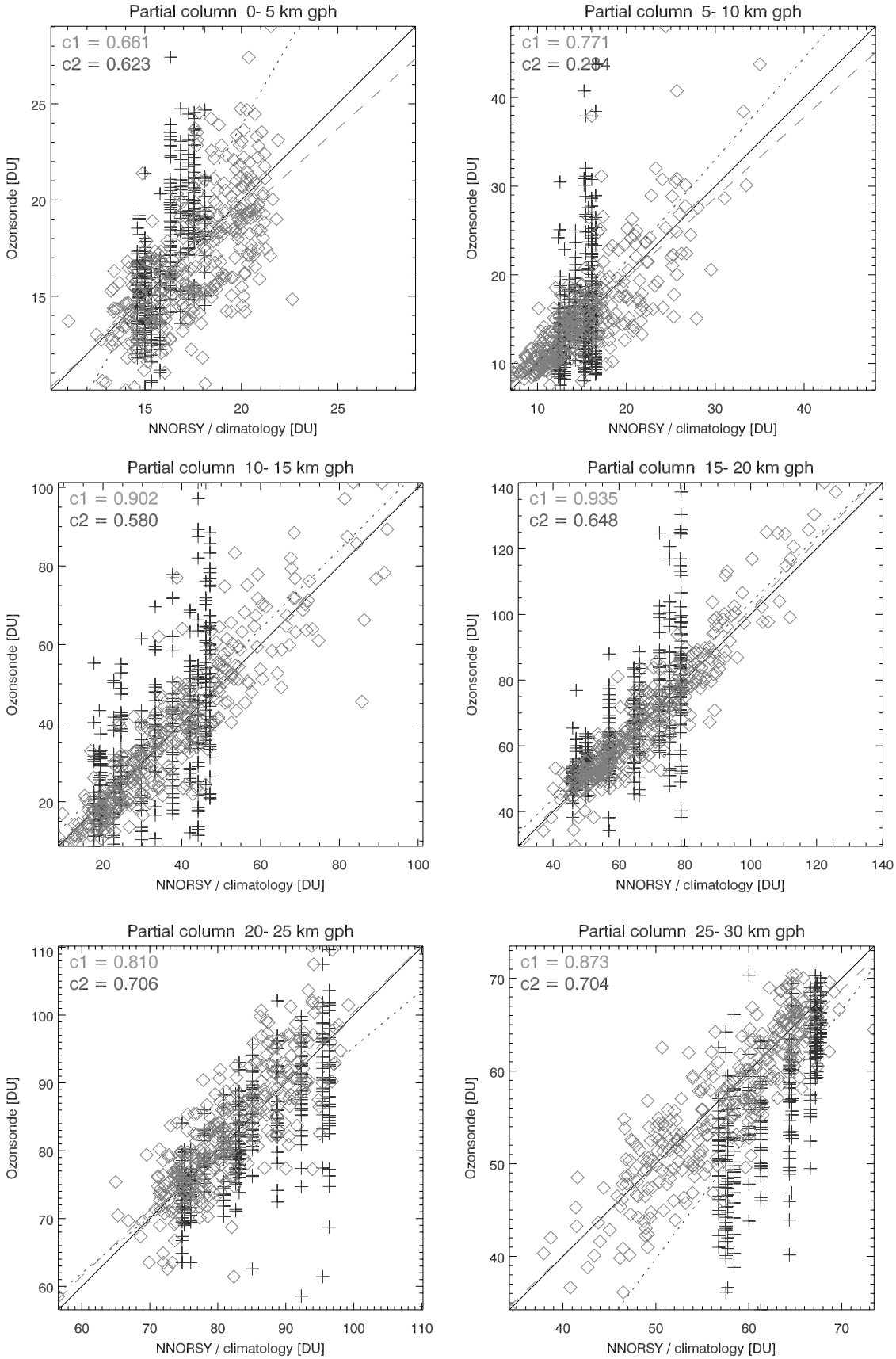

Figure 6. Scatterplots of NNORSY versus Hohenpeissenberg ozonesondes (diamonds) and the FK climatology versus sondes (pluses). Here, c1 is the Pearson correlation for NNORSY, and c2 is for FK. Regression curves are printed dashed and dotted, respectively. See color version of this figure at back of this issue.

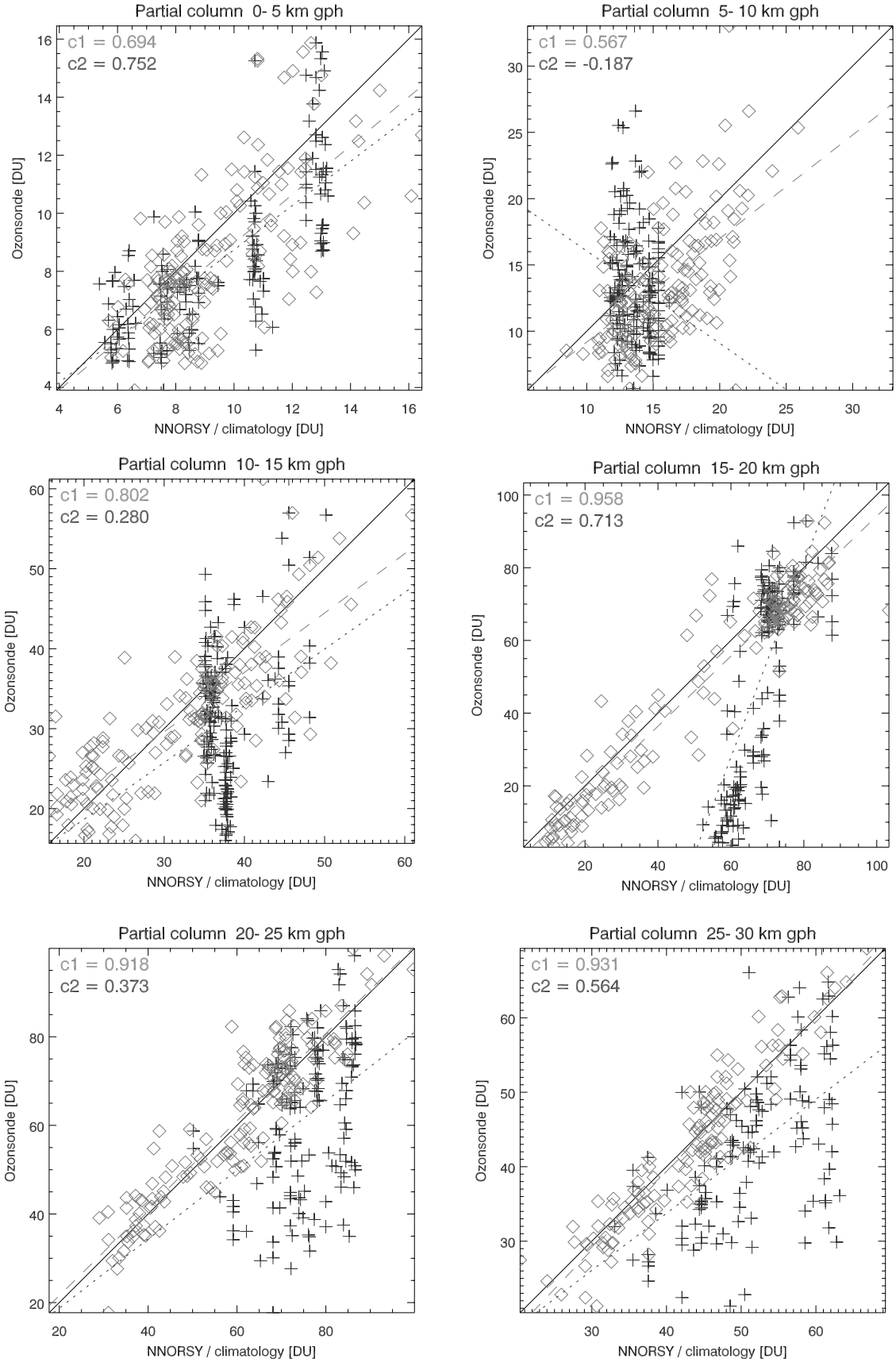

Figure 7. Same as Figure 6, but for station Syowa (69.0°S, 39.6°E). See color version of this figure at back of this issue.

wavelengths beyond the 325 nm retrieval range boundary. However, extending the wavelength range to 335 or 340 nm lead to slightly larger errors globally, and it is probable that the S/N ratio of the measurement would not allow accurate retrievals in this region anyway [*Manney et al.*, 2001]. Above 10 km, NNORSY does pick up the ozone dynamics fairly well. The sharp distinction between ozone hole condition and unperturbed ozone profiles can be seen clearly in the 15 to 20 km layer average, where the data points are divided into two different clusters. It also seems that the climatology is systematically overestimating ozone values under ozone hole conditions, while maximum values agree very well with sondes. The same applies to a somewhat lesser degree to adjacent height layers. This is another direct indication of the deepening of the ozone hole compared to the 1980s as represented by the FK climatology.

[43] The timeline plots for Syowa (not shown) are qualitatively comparable to the ones from Hohenpeissenberg; that is, largest deviations of NNORSY from the sondes occur under condition of high ozone variability. A positive bias of +3 DU (12%) exists in the lowest 10 km layer and of +5 DU (6%) in the middle layer. Bias and standard deviations do not notably change over time.

5.4. Arctic Ozone Depletion

[44] We now switch to the northern hemisphere by qualitatively comparing a partial GOME orbit to retrievals with the FURM method. *Eichmann et al.* [1999] have thoroughly investigated a specific Arctic ozone hole situation which occurred on 2 April 1997. In a period lasting almost three weeks, low temperatures induced the formation of Type I polar stratospheric clouds inside the polar vortex [*Coy et al.*, 1997] that in turn led to massive chemical ozone destruction [*Müller et al.*, 1997].

[45] Figure 8a is a compilation of NNORSY ozone profiles from 120 nadir pixels along GOME orbit 10197, plotted against latitude. The same situation is depicted in Figure 8b as retrieved with the FURM v5 algorithm, where clusters of eight pixels are coadded prior to retrieval. While there is good agreement between the two retrieval methods up to 63 N, the northward decline of ozone concentration seems to be stronger in the NNORSY data. Figure 9 shows three distinct NNORSY profiles from orbit 10197 at different latitudes, with collocated ozonesonde measurements. The neural network slightly exaggerates the ozone concentration in the lower stratosphere at Payerne, and smoothes out part of the steep tropopause flank at Lervick, however tropopause height is correctly retrieved. At Sodankyla, the total ozone content agrees very well with the sonde, but part of the lower stratospheric ozone is shifted upward to fill the hole around 15 km, such that the two-layer structure is not detected.

5.5. Integrated Ozone Columns

[46] We have shown so far that the NNORSY ozone profiles compare well against sondes and OE-based retrievals on a small spatial scale. In order to check the global validity of the data, integrated monthly mean ozone columns have been calculated globally, and compared to total ozone measurements from other sources. The Total Ozone Mapping Spectrometer (TOMS) version 7 (v7) data [*McPeters et al.*, 1998] have been chosen as a reference for total ozone.

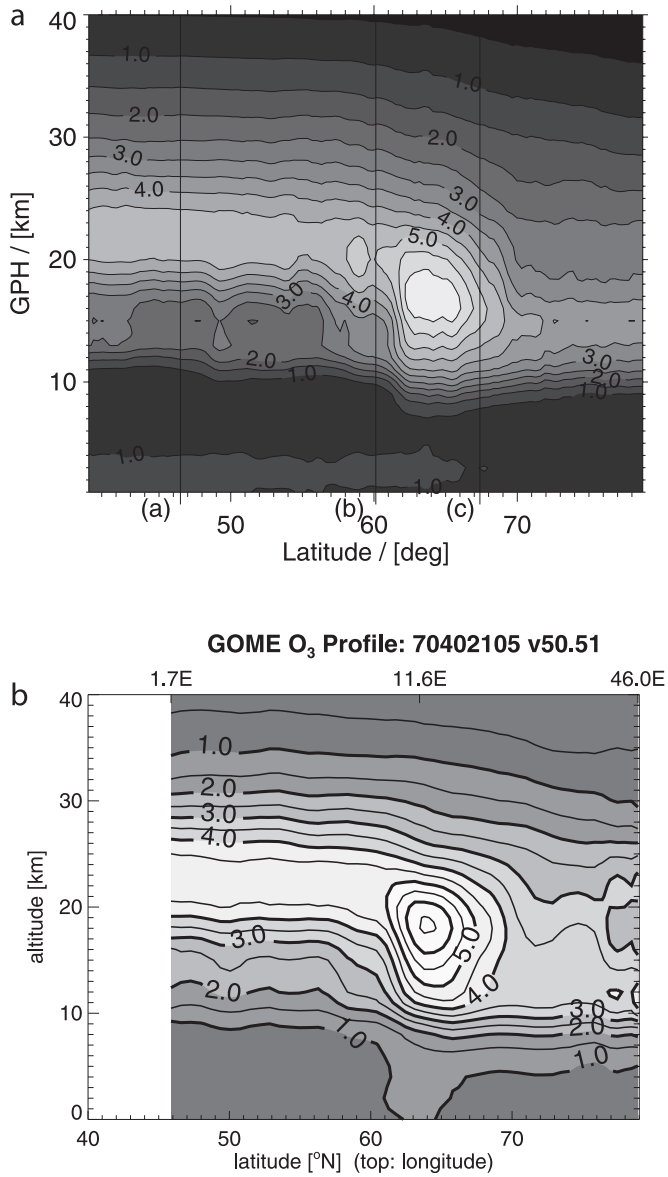

Figure 8. Ozone depletion in the polar vortex as seen from GOME, part of orbit 10197 on 2 April 1997. (a) NNORSY ozone profile retrieval. Vertical lines refer to sonde collocations in Figure 9. (b) FURM v5, updated from *Eichmann et al.* [1999].

Bodeker et al. [2001] derived a climatological correction function for TOMS v7 ozone columns to make the data more consistent with ground stations. There is some discussion as to whether this draws TOMS closer to the (unknown) true ozone field, but the correction has been found to yield an improvement of results when training neural networks to derive total ozone from TIROS Operational Vertical Sounder (TOVS) [*Kaifel and Müller*, 2001; *Müller and Kaifel*, 1999] and GOME data [*Müller et al.*, 2001, 2002]. The correction is a parameterized function of time, season and latitude, reaching its maximum of around −20 DU in the SH summer, with values ranging between 0 and −10 DU for most other times and latitudes.

[47] Figure 10 shows the monthly average TOMS ozone field with the aforementioned correction applied, and its

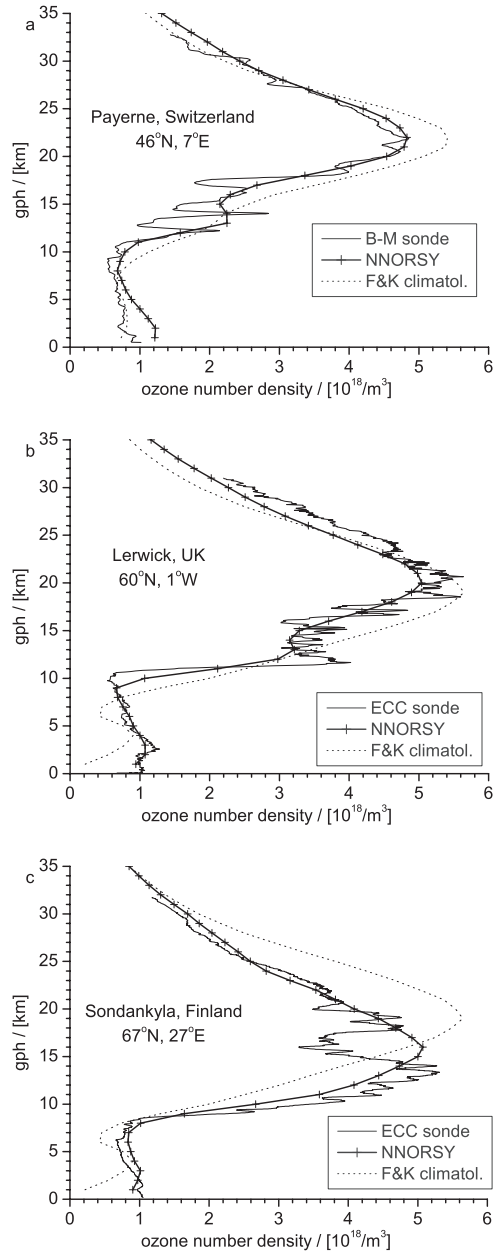

Figure 9. Sonde collocations for the GOME orbit depicted in Figure 8.

difference to integrated NNORSY profiles. Some features exhibited in these maps are quite characteristic for the method and occur on monthly difference plots for other years and months as well (not shown).

[48] Area-weighted, global biases between the ozone fields tend to be minimal, while local differences are generally lower than 20–30 DU. NNORSY seems to have a tendency to underestimate the ozone maximum, while it overestimates ozone in the ozone hole area. This seems to be a property of the trained neural network: Since extreme values are generally less likely than average values, the networks tends to adjust the distribution of output profiles toward the mean, thereby cropping the edges of the distribution somewhat. However, the effect is not very pronounced, otherwise a strong tilt of the NNORSY regression curve toward the vertical would be present in Figures 6 and 7. Similar plots for the limb sounders (not shown) do indeed reveal a slight tilt in the case of SAGE, the magnitude of which would explain the slight underestimation over the SH oceans.

[49] Note also that the neural network does not receive any information about ground elevation. We have tried including such into the input data, but the results did not noticeably improve. Therefore a high bias over high terrain, such as Antarctica or the Himalaya, should be partially compensated for if ozone values retrieved "below the ground" are removed prior to total column integration using a digital elevation model.

[50] Last but not least, the solar zenith angle issue which already surfaced in sections 4.2 and 5.3 shows in the maps as absolute highest deviations from TOMS of more that 30 DU, close to the polar terminator. This problem is rooted in the lack of training data around the poles: There is no occultation data north of 71°N, and almost no sonde data from the SH oceans, which may lead to an inaccurate climatological representation of the average ozone field in the neural network. Also, since the polar latitudes are only sunlit during part of the year, collocations in these regions are likely to be always underrepresented in the data set. Several methods to overcome these problems are currently being investigated.

[51] Overall, the offsets with respect to monthly TOMS ozone fields are thus of the order of 0–5% globally, with maxima of the order of 5–10% in medium to high-ozone conditions, and around 10–20% in low-ozone conditions. Even better agreement has been achieved with a neural network trained on GOME collocations with total ozone data. Further discussion on this model and the total ozone comparisons can be found in [*Müller et al.*, 2002]. The findings are generally in line with a comprehensive analysis of TOMS, TOVS and GOME ozone field differences provided by *Corlett and Monks* [2001].

6. Conclusions

[52] It has been demonstrated that the regularization imposed by using a neural network approach is sufficient to solve the inverse retrieval problem for GOME ozone profiles. The results are comparable to classical methods, with possibly better horizontal and vertical resolution. NNORSY is currently taking part in the international effort of comparing different retrieval systems in the framework of the European Space Agency (ESA) GOME Ozone Profiling Working Group, where we expect to gain more insight into the potential of our method. First comparisons within this group did show very promising results.

[53] One advantage of NNORSY is speed, making it well suited for real-time applications and global data reprocessing, even at full GOME horizontal resolution. A prototype near real-time system is already in operation at the German Remote Sensing Datacenter (DFD) of the DLR, the data can be accessed via the Internet (http://auc.dfd.dlr.de/GOME_NRT/profile.html).

[54] The proposed method is implicitly correcting for cloud albedos and degradation in GOME channels, therefore it can be employed in cases where explicitly modeling radiative transport, and/or accurately calibrating the mea-

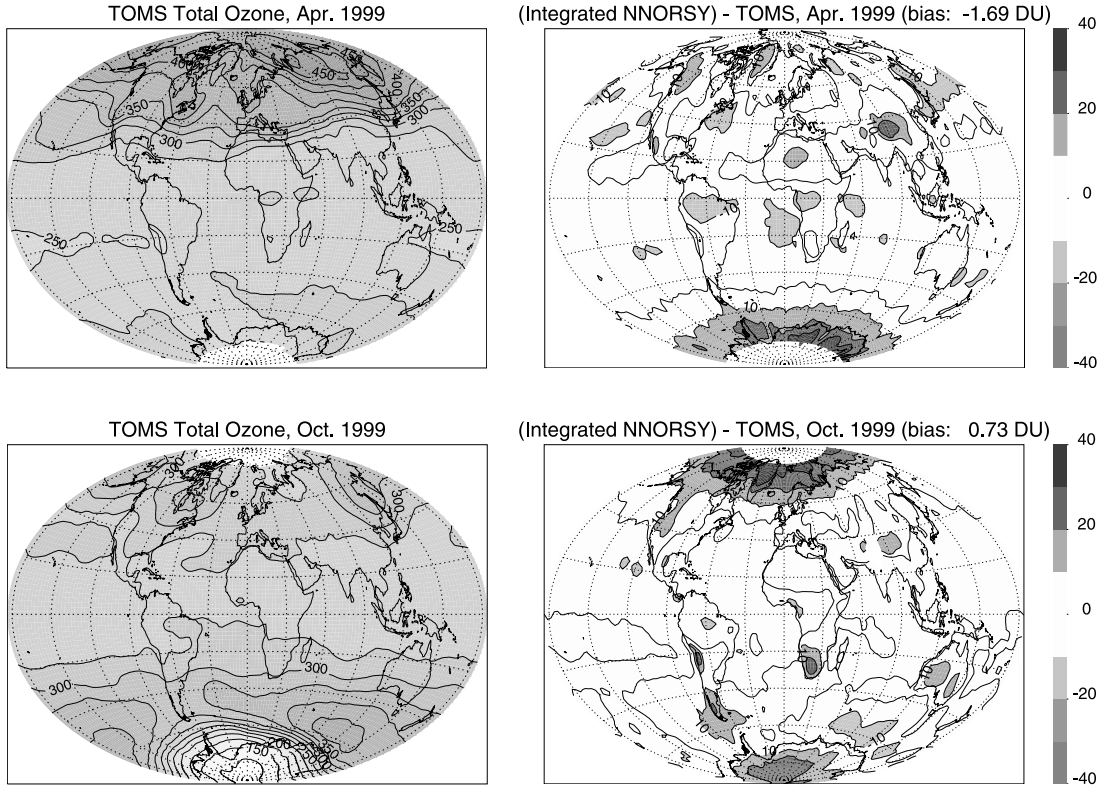

Figure 10. Monthly mean comparison of TOMS v7 total ozone with integrated NNORSY ozone profiles. All scales in DU. See color version of this figure at back of this issue.

surements is otherwise difficult to achieve. There is not even a need for a forward model.

[55] On the other hand, NNORSY cannot be used in its current form for species that are only sparsely measured because of the training data requirements. However, if a forward model can accurately simulate measurements for a given sensor, using a partially or entirely simulated training data set is a viable option. In fact, this approach has recently led to the development of a new type of ground-based UV spectral radiometer (http://www.sprafimo.de) based entirely on simulated UV ground spectra [*Schwander et al.*, 2001].

[56] For NNORSY-GOME ozone profiles, further improvements in the fields of spectral calibration and state space sampling distribution could lead to a yet better data quality in the future, especially concerning extreme cases of ozone profiles. A definite improvement can be expected from combining different specialist networks in a controlled way. Future work will also focus on exploiting additional profile data sources and on improving the outlier detection algorithms for both ozone training data and GOME spectra.

[57] An adaptation of the method toward state of the art sensors (SCIAMACHY, OMI, GOME-2) is planned, and can be carried out with considerably reduced effort, since instrument calibration specifics are learned automatically by the network, and much of the work in setting up software and training data has already been done. Since both the number of available training data and the computational effort for classical retrieval and/or assimilation of data from upcoming satellite instruments increase steadily, we expect to see growing use of neural network type methods in satellite meteorology, especially in the operational regime. Conceivable applications include other trace gases, temperature profiles, accurate forward model emulation, data assimilation assistance and alternative measurement techniques.

Appendix A: Neural Networks in the Retrieval Context

[58] Let $\mathbf{x} = (x_1, x_2, \ldots, x_n)^t$ be the discretized state of the atmosphere at a certain geographical location, and $\mathbf{y} = (y_1, y_2, \ldots, y_m)^t$ the corresponding satellite-measured top-of-atmosphere radiances. In retrieval theory [e.g., *Rodgers*, 1990], it is assumed for physical reasons that the relationship between $\mathbf{x}$ and $\mathbf{y}$ can be modeled as

$$\mathbf{y} = \mathbf{F}(\mathbf{x}, \mathbf{b}) + \boldsymbol{\epsilon}, \tag{A1}$$

where $\mathbf{F}$ is a (radiative transfer) forward model depending on the atmospheric state $\mathbf{x}$ and a number of additional parameters which are for simplicity combined into one vector $\mathbf{b}$. The measurement noise vector $\boldsymbol{\epsilon}$ is assumed to have Gaussian statistics. In general, the model $\mathbf{F}$ will not be linear, but since it represents a continuous function, it can be linearized in the vicinity of a certain state $\mathbf{x}_0$, such that

$$\mathbf{y} - \mathbf{F}(\mathbf{x}_0) = \left.\frac{\partial \mathbf{F}}{\partial \mathbf{x}}\right|_{\mathbf{x}_0} (\mathbf{x} - \mathbf{x}_0) + \mathcal{O}(\mathbf{x}^2) \approx \mathbf{K}(\mathbf{x} - \mathbf{x}_0), \tag{A2}$$

where $K = \frac{\partial \mathbf{F}}{\partial \mathbf{x}}$ is called the kernel matrix. Usually, the rank of $\mathbf{K}$ is smaller than the state space dimension n, which leads to a manifold of possible solutions $\mathbf{x}$ for any given

observation $\mathbf{y}$ [*Rodgers*, 2000]. It is therefore reasonable to look at the problem from a Bayesian point of view: The most probable solution $\hat{\mathbf{x}}$ is the one that maximizes the likelihood $\mathcal{L} = p(\mathbf{x}|\mathbf{y})$, with $p(\mathbf{x}|\mathbf{y})$ denoting the conditional probability density of $\mathbf{x}$ given the observation $\mathbf{y}$. This is equivalent to minimizing an error function

$$E = -\ln \mathcal{L} = -\ln p(\mathbf{x}|\mathbf{y}) = -\ln\left(\frac{p(\mathbf{y}|\mathbf{x})p(\mathbf{x})}{p(\mathbf{y})}\right)$$
$$= (\mathbf{y}-\mathbf{K}\mathbf{x})^t\mathbf{S}_e^{-1}(\mathbf{y}-\mathbf{K}\mathbf{x}) + (\mathbf{x}-\mathbf{x}_a)^t\mathbf{S}_a^{-1}(\mathbf{x}-\mathbf{x}_a) + const., \tag{A3}$$

where Bayes' theorem was used in the first line and the assumption of Gaussian errors in the second. The covariance matrix $\mathbf{S}_e$ contains forward model and measurement errors, while $\mathbf{S}_a$ tries to model the natural variability of the state, centered around some a priori $\mathbf{x}_a$.

[59] Since we assumed Gaussian distribution for all errors involved, it follows that $p(\mathbf{x}|\mathbf{y})$ is also a Gaussian. This function can be sampled using a set of observations $\{\mathbf{y}^p\}$, $p \in \{1, \ldots, T\}$, for which the corresponding states $\mathbf{x}^p$ are known. Under the assumption of the existence of an inverse radiative transfer function defined by equation (1), we can write the error function as

$$E = -\ln \prod_{p=1}^{T} p(\mathbf{x}^p|\mathbf{y}^p) =$$
$$= \sum_{p=1}^{T} (\mathbf{R}(\mathbf{y}^p, \mathbf{c}^p, \mathbf{w}) - \mathbf{x}^p)^t \hat{\mathbf{S}}^{-1} (\mathbf{R}(\mathbf{y}^p, \mathbf{c}^p, \mathbf{w}) - \mathbf{x}^p), \tag{A4}$$

whereby the constant terms have been omitted. The vector c roughly corresponds to b from equation (A1), but may contain additional parameters not needed for forward calculation. In practice, when using a feed forward neural network to model $\boldsymbol{R}$, equation (A4) is often simplified for computational reasons by assuming $\hat{\mathbf{S}} = \sigma^2\mathbf{I}_n$ for all training pairs. (Suitable normalization of $\boldsymbol{y}$ within the preprocessing step ensures that the output variances are all in the same order of magnitude.) The constant σ can then be omitted from the error function, which leads to equation (2).

[60] The neural network employed here consists of a one-dimensional input layer containing enough nodes (neurons) to receive the input $\mathbf{y}$ and $\mathbf{c}$. Each input node is connected to all nodes of a second, hidden layer of neurons via synapses carrying weights $\mathbf{w}$. When presented with an input data vector, the input signals propagate along the synapses while being multiplied by the weights. The hidden neurons essentially sum up all incoming signals, and use a fixed nonlinear function, in our case tanh, to in turn define their outputs, which propagate through another layer of weighted synapses to the output neurons. These neurons again sum up their inputs and use another tanh transfer function and a suitable renormalization to define the network output $\mathbf{x}$. (This step also serves to regularize the method by constraining the output profile to physically meaningful values, here chosen to be greater than zero and less than a long-term maximum plus a safety margin.) Thus the network is essentially a mapping from measurement space to state space parameterized by means of the weights $\mathbf{w}$.

[61] **Acknowledgments.** We are grateful to the IUP staff for their knowledgeable help concerning the GOME sensor. We thank G. Bodeker (NIWA) for providing us with the coefficients for the correction of TOMS data with respect to the Dobson network, and E. Hare (WOUDC) for support with the WOUDC data archive. This work would not have been possible without the effort of the those doing the thousands of ozone soundings used, to whom we feel deeply indebted. We also wish to thank the PIs and providers of free and simple access to SAGE, HALOE, POAM and SHADOZ data. This project is funded by the Bundesministerium für Bildung und Forschung (BMBF) under contract number 50EE995 (at IUP) and 50EE996 (at ZSW).

References

Aires, F., C. Prigent, W. B. Rossow, and M. Rothstein, A new neural network approach including first guess for retrieval of atmospheric water vapor, cloud liquid water path, surface temperature, and emissivities over land from satellite microwave observations, *J. Geophys. Res.*, *106*, 14,887–14,908, 2001.

Baron, A., Approximation and estimation bound for artificial neural networks, *Mach. Learning*, *14*, 115–133, 1994.

Bishop, C. M., *Neural Networks for Pattern Recognition*, Clarendon, Oxford, UK, 1995.

Bodeker, G. E., J. C. Scott, K. Kreher, and R. L. McKenzie, Global ozone trends in potential vorticity coordinates using TOMS and GOME intercompared against the dobson network: 1978–1998, *J. Geophys. Res.*, *106*, 23,029–23,042, 2001.

Bovensmann, H., J. P. Burrows, M. Buchwitz, J. Frerick, S. Noel, V. Rozanov, K. V. Chance, and A. H. P. Goede, SCIAMACHY—Mission objectives and measurement modes, *J. Atmos. Sci.*, *56*, 125–150, 1999.

Burrows, J., E. Hölzle, A. Goede, H. Visser, and W. Fricke, SCIAMACHY—Scanning Imaging Absorption Spectrometer for Atmospheric Chartography, *Acta Astronaut.*, *35*, 445–451, 1995.

Burrows, J., et al., Global Ozone Monitoring Experiment (GOME): Mission concept and first scientific results, *J. Atmos. Sci.*, *56*, 151–175, 1999.

Chevallier, F., F. Chéruy, N. A. Scott, and A. Chédin, A neural network approach for a fast and accurate computation of a longwave radiative budget, *J. Appl. Meteorol.*, *37*, 1385–1397, 1998.

Corlett, G. K., and P. S. Monks, A comparison of total column ozone values derived from the Global Ozone Monitoring Experiment (GOME), the Tiros Operational Vertical Sounder (TOVS), and the Total Ozone Mapping Spectrometer (TOMS), *J. Atmos. Sci.*, *58*, 1103–1116, 2001.

Coy, L., E. Nash, and P. Newman, Meteorology of the polar vortex: Spring 1997, *Geophys. Res. Lett.*, *24*, 2693–2696, 1997.

Cunnold, D. M., W. P. Chu, R. A. Barnes, M. P. McCormick, and R. E. Veiga, Validation of SAGE II ozone measurements, *J. Geophys. Res.*, *94*, 8447–8460, 1989.

Cunnold, D. M., H. J. Wang, L. W. Thomason, J. M. Zawodny, J. A. Logan, and I. A. Megretskaia, SAGE (version 5.96) ozone trends in the lower stratosphere, *J. Geophys. Res.*, *105*, 4445–4457, 2000.

de Beek, R., Bestimmung von Ozonvertikalprofilen aus Messungen des Satelliteninstrumentes GOME im ultravioletten und sichtbaren Spektralbereich (in German), *Ber. Umweltphys. D46*, Inst. of Environ. Phys., Univ. of Bremen, Bremen, Germany, 1998.

de Beek, R., R. Hoogen, V. Rozanov, and J. Burrows, Ozone profile retrieval from GOME satellite data I: Algorithm description, in *Space at the Service of our Environment*, vol. II, *ESA SP-414*, edited by T.-D. Guyenne and D. Danesy, pp. 749–754, Eur. Space Agency, Noordwijk, Netherlands, 1997.

Deniel, C., et al., A comparative study of POAM II and ECC sonde ozone measurements obtained over northern Europe, *J. Geophys. Res.*, *102*, 23,629–23,642, 1997.

Eichmann, K.-U., K. Bramstedt, M. Weber, V. V. Rozanov, R. Hoogen, and J. P. Burrows, O_3 profiles from GOME satellite data - II: Observations in the Arctic spring 1997 and 1998, *Phys. Chem. Earth*, *24*, 453–457, 1999.

Fortuin, J. P. F., and H. Kelder, An ozone climatology based on ozonesonde and satellite measurements, *J. Geophys. Res.*, *103*, 31,079–31,734, 1998.

Hasekamp, O., J. Landgraf, F. Helmich, R. van Oss, and R. van der A, Two inversion methods for ozone profile retrieval from GOME, in *ESAMS'99—European Symposium on Atmospheric Measurements from Space, PP-161*, pp. 549–553, Eur. Space Agency, Noordwijk, Netherlands, 1999.

Hoogen, R., V. Rozanov, R. de Beek, K. Bramstedt, K.-U. Eichmann, M. Weber, M. Buchwitz, T. Kurosu, and J. P. Burrows, Ozone profiles from GOME satellite data - Part I: Advances in retrieval algorithm development, paper presented at Fourth European Symposium on Stratospheric Ozone Research, Eur. Space Agency, Schliersee, Germany, 1997.

Hoogen, R., V. V. Rozanov, and J. P. Burrows, Ozone profiles from GOME satellite data: Algorithm description and first validation, *J. Geophys. Res.*, *104*, 8263–8280, 1999.

Hornik, K., M. Sinchcombe, and H. White, Multilayer feedforward networks are universal approximators, *Neural Networks*, *2*, 359–366, 1989.

Jiménez, C., Inversion of microwave limb sounding observations of the atmosphere by a neural network technique, *Tech. Rep. 364L*, Dept. Radio and Space Sci., Chalmers Univ. of Technol., Göteborg, Sweden, 2000.

Kaifel, A. K., and M. D. Müller, Results of neural network total ozone retrieval on global NOAA-TOVS data, in *Technical Proceedings of the 10th International ATOVS Study Conference, Boulder CO, USA, 27th January–2nd February 1999*, edited by J. F. Le Marshall and J. D. Jasper, pp. 262–275, Bur. of Meteorol. Res. Cent., Melbourne, Victoria, Australia, 1999.

Kaifel, A. K., and M. D. Müller, Results of TOVS ozone retrieval with neural networks, in *Technical Proceedings of the 11th International ATOVS Study Conference, Budapest, Hungary, 20–26 September 2000*, edited by J. Le Marshall and J. D. Jasper, pp. 153–165, Bur. of Meteorol. Res. Cent., Melbourne, Victoria, Australia, 2001.

Kerr, J. B., et al., The 1991 WMO international ozonesonde intercomparison at Vanscoy, Canada, *Atmos. Ocean.*, *32*, 685–716, 1994.

Krasnopolsky, V. M., Neural networks for standard and variational satellite retrievals, *OMB Contrib. 148*, NOAA Environ. Model. Cent., Ocean Model. Branch, Washington, D.C., 1997.

Lawrence, S., A. D. Back, A. C. Tsoi, and C. L. Giles, On the distribution of performance from multiple neural-network trials, *IEEE Trans. Neural Networks.*, *8*, 1507–1517, 1997.

Lelieveld, J., and F. J. Dentener, What controls tropospheric ozone?, *J. Geophys. Res.*, *105*, 3531–3551, 2000.

Lu, J., V. A. Mohnen, G. K. Yue, R. J. Atkinson, and W. A. Matthews, Intercomparison of stratospheric ozone profiles obtained by SAGE II, HALOE, and ozonesondes during 1994–1995, *J. Geophys. Res.*, *102*, 16,137–16,144, 1997.

Lucke, R. L., et al., Polar Ozone and Aerosol Measurement (POAM) III instrument and early validation results, *J. Geophys. Res.*, *104*, 18,785–18,799, 1999.

Lumpe, J. D., R. M. Bevilacqua, K. W. Hoppel, and C. E. Randall, POAM III retrieval algorithm and error analysis, *J. Geophys. Res.*, *107*(D21), 4575, doi:10.1029/2002JD002137, 2002.

Manney, G. L., et al., Comparison of satellite ozone observations in coincident air masses in early November 1994, *J. Geophys. Res.*, *106*, 9923–9944, 2001.

McPeters, R. D., et al., Earth probe total ozone mapping spectrometer (TOMS) data products user's guide, *NASA Tech. Publ., 1998-206895*, 70 pp., 1998.

Müller, M. D., Bestimmung von atmosphärischem Gesamtozon und Ozonprofilen aus GOME Daten mit Hilfe des Neural Network Ozone Retrieval System (NNORSY) (in German), Ph. D., thesis, Inst. of Environ. Phys., Univ. of Bremen, Bremen, Germany, 2002.

Müller, M. D., and A. K. Kaifel, Efficient processing of multi-year global TOVS data using ITPP, 3I and neural networks, in Technical Proceedings of the 11th International ATOVS Study Conference, Boulder CO, USA, 27th January–2nd February 1999, edited by J. F. Le Marshall and J. D. Jasper, pp. 397–407, Bur. of Meteorol. Res. Cent., Melbourne, Australia, 1999.

Müller, M. D., A. K. Kaifel, and M. Weber, Ozone from GOME data using neural network technique, in *Proceedings of ERS-Envisat Symposium, Gothenburg, Sweden, 16–20 October 2000, Spec. Publ. SP-461*, edited by H. Sawaya-Lacoste, ESA Publ. Div., Eur. Space Agency–Eur. Space Res. and Technol. Cent., Noordwijk, Netherlands, 2001.

Müller, M. D., A. Kaifel, M. Weber, and J. P. Burrows, Neural network scheme for the retrieval of total ozone from Global Ozone Monitoring Experiment data, *Appl. Opt.*, *41*, 5051–5058, 2002.

Müller, R., J.-U. Grooß, D. McKenna, P. Crutzen, C. Brühl, J. M. Russell, and A. Tuck, HALOE observations of the vertical structure of chemical ozone depletion in the Arctic vortex during winter and early spring 1996–1997, *Geophys. Res. Lett.*, *24*, 2717–2720, 1997.

Papadopoulos, G., P. J. Edwards, and A. F. Murray, Confidence estimation methods for neural networks: A practical comparison, *IEEE Trans. Neural Networks*, *12*, 1278–1287, 2001.

Reid, S. J., and G. Kiladis, On the changing abundance of ozone minima at northern midlatitudes, *J. Geophys. Res.*, *105*, 12,169–12,180, 2000.

Riedmiller, M., and H. Braun, A direct adaptive method for faster backpropagation learning: The Rprop algorithm, paper presented at International Conference on Neural Networks, Inst. of Electr. and Electr. Eng., San Francisco, Calif., 1993.

Rodgers, C. D., Retrieval of atmospheric temperature and composition from remote measurements of thermal radiation, *Rev. Geophys.*, *14*, 609–624, 1976.

Rodgers, C. D., Characterisation and error analysis of profiles retrieved from remote sounding measurements, *J. Geophys. Res.*, *95*, 5587–5595, 1990.

Rodgers, C. D., *Inverse Methods for Atmospheric Sounding: Theory and Practice*, World Sci., River Edge, N.J., 2000.

Rozanov, V., D. Diebel, R. J. D. Spurr, and J. P. Burrows, GOMETRAN: A radiative transfer model for the satellite project GOME, The plane-parallel version, *J. Geophys. Res.*, *102*, 16,683–16,695, 1997.

Rumelhart, D. E., G. Hinton, and R. Williams, Learning internal representations by error backpropagation, in *Parallel Distributed Processing*, vol. 1, edited by D. Rumelhart and J. McClellant, pp. 318–362, MIT Press, Cambridge, Mass., 1986.

Russell, L. J., et al., The halogen occultation experiment, *J. Geophys. Res.*, *98*, 10,777–10,797, 1993.

Schwander, H., A. Kaifel, A. Ruggaber, and P. Koepke, Spectral radiative-transfer modeling with minimized computation time by use of a neural-network technique, *Appl. Opt.*, *40*, 331–335, 2001.

Siddans, R. W., B. J. Kerridge, J. Reburn, A. Stevens, and R. Munro, Height-resolved ozone retrievals spanning the troposphere and stratosphere from GOME, in *ESAMS'99-European Symposium on Atmospheric Measurements from Space, Noordwijk, Netherlands, 18–22 January 1999, WPP-161*, pp. 299–305, Eur. Space Agency, Noordwijk, 1999.

Singer, S. F., and R. C. Wentworth, A method for the determination of the vertical ozone distribution from a satellite, *J. Geophys. Res.*, *62*, 299–308, 1957.

Stratospheric Processes and Their Role in Climate (SPARC), SPARC/IO_3C/GAW assessment of trends in the vertical distribution of ozone, *WCRP-SPARC Rep. WMO Tech. Doc. 935*, World Meteorol. Org., Geneva, 1998.

Steele, H. M., and R. P. Turco, Separation of aerosol and gas components in the Halogen Occultation Experiment and the Stratospheric Aerosol and Gas Experiment (SAGE) II extinction measurements: Implications for SAGE II ozone concentrations and trends, *J. Geophys. Res.*, *102*, 19,665–19,681, 1997.

Swinbank, R., and A. O'Neill, A stratosphere-troposphere data assimilation system, *Mon. Weather*, 122, 1994.

Thompson, A. M., et al., Southern Hemisphere Additional Ozonesondes (SHADOZ) 1998–2000 tropical ozone climatology, 1, Comparison with Total Ozone Mapping Spectrometer (TOMS) and ground-based measurements, *J. Geophys. Res.*, *108*(D2), 8238, doi:10.1029/2001JD000967, 2003.

van der A, R., Ozone profile retrieval and its application to the polar view mode of GOME, in *ESAMS'99-European Symposium on Atmospheric Measurements from Space, Noordwijk, Netherlands, 18–22 January 1999, WPP-161*, pp. 295–298, Eur. Space Agency, Noordwijk, Netherlands, 1999.

van der A, R. J., A. J. M. Piters, R. F. van Oss, P. J. M. Valks, J. H. G. M. van Geffen, H. M. Kelder, and C. Zehner, Near-real time delivery of GOME ozone profiles, in *Proceedings of ERS-Envisat Symposium, Gothenburg, Sweden, 16–20 October 2000, Spec. Publ. SP-461*, edited by H. Sawayah-Lacoste, ESA Publ. Div., Eur. Space Agency–Eur. Space Res. and Technol. Cent., Noordwijk, Netherlands, 2001.

van Oss, R. F., and R. Spurr, Fast and accurate ozone profile retrieval for GOME-2 using 4-stream LIDORT, in *Proceedings of ERS-Envisat Symposium, Gothenburg, Sweden, 16–20 October 2000, Spec. Publ. SP-461*, edited by H. Sawaya-Lacoste, ESA Publ. Div., Eur. Space Agency–Eur. Space Res. and Technol. Cent., Noordwijk, Netherlands, 2001.

Wardle, D. I., E. W. Hare, D. V. Barton, and C. T. McElroy, Atmospheric ozone, in *Proceedings of the XVIII Quadrennial Ozone Symposium, L'Aquila, Italy, 12–21 September 1996*, edited by R. Bojkov and G. Visconti, Int. Ozone Comm., Athens, Greece, 1998.

J. P. Burrows, S. Tellmann, and M. Weber, Institute of Environmental Physics (IUP), University of Bremen FB1, P.O. Box 330440, 28334 Bremen, Germany. (john.burrows@iup.physik.uni-bremen.de; silvia.tellmann@iup.physik.uni-bremen.de; mark.weber@iup.physik.uni-bremen.de)

A. K. Kaifel and M. D. Müller, Center for Solar Energy and Hydrogen Research (ZSW) Industriestraße 6, 70565 Stuttgart, Germany. (anton.kaifel@zsw-bw.de; martin.mueller@zsw-bw.de)

D. Loyola, Remote Sensing Technology Institute (IMF), German Aerospace Center (DLR), DLR Oberpfaffenhofen, 82234 Weßling, Germany. (Diego.Loyola@dlr.de)

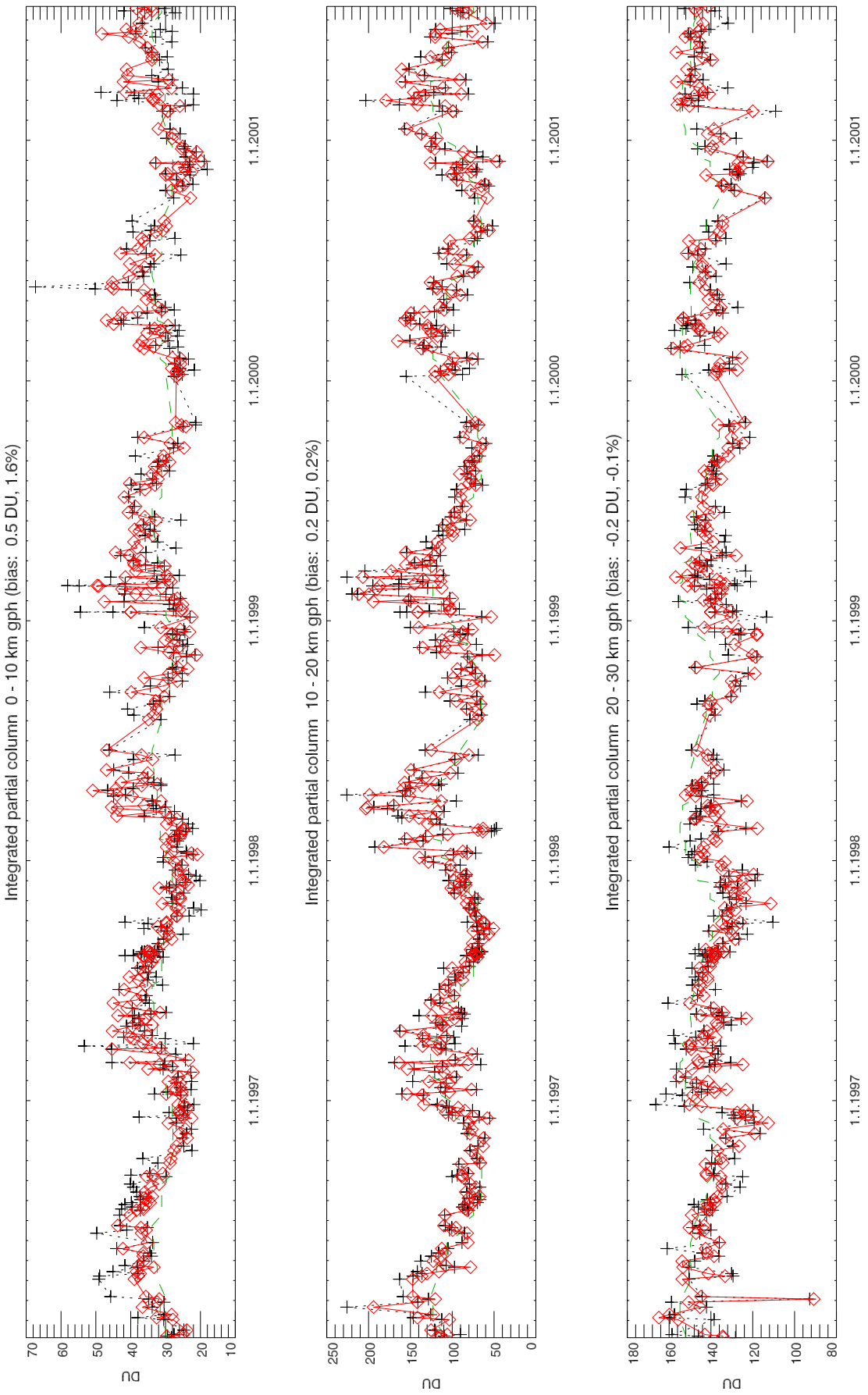

Figure 5. Timeline of partial ozone columns from NNORSY (diamonds) and collocated Hohenpeissenberg (47.8°N, 11.0°E) ozone sondes (pluses). Multiple collocations within 160 km were averaged into single points. The FK climatology is plotted for comparison as a dashed curve.

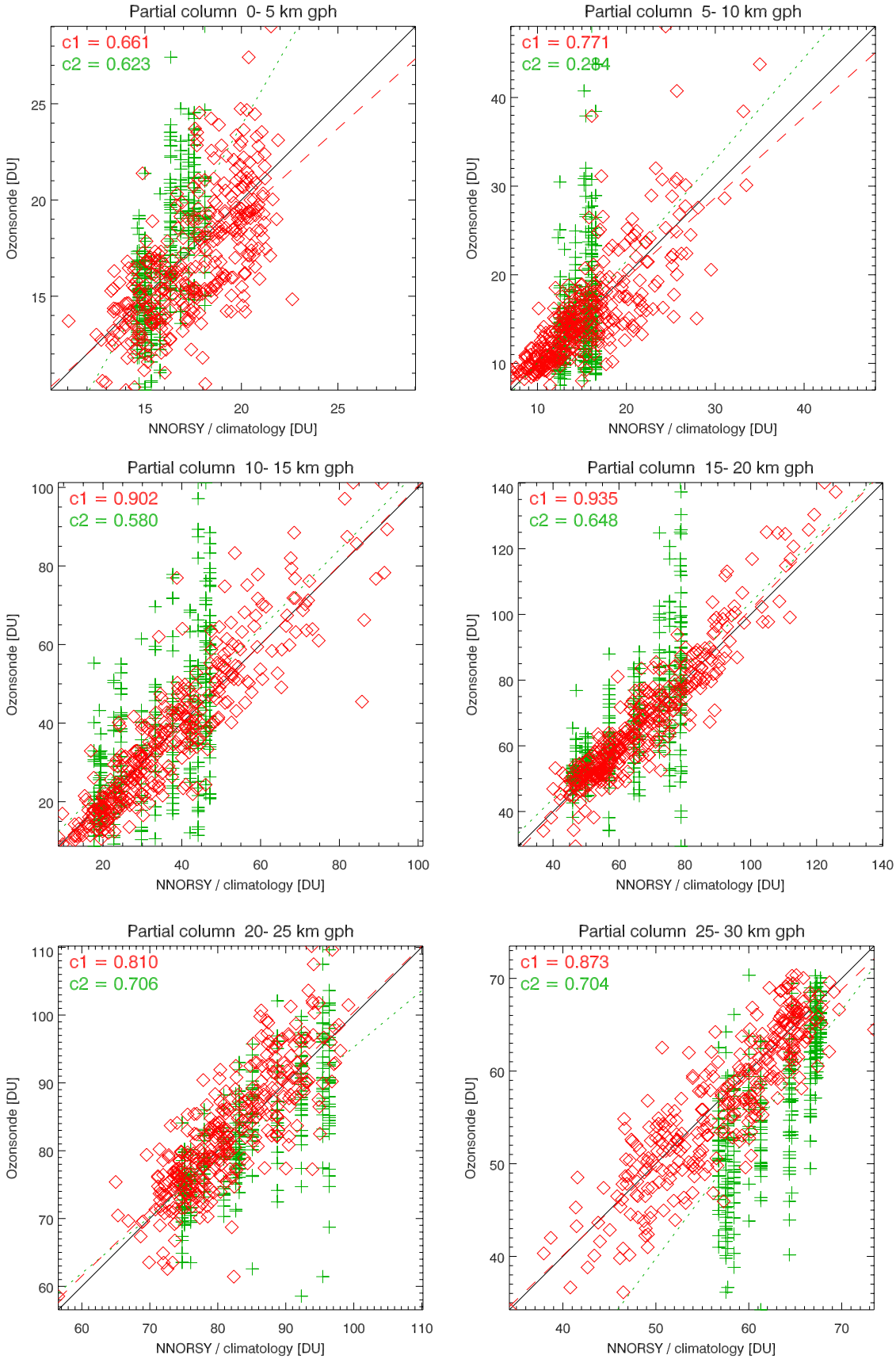

Figure 6. Scatterplots of NNORSY versus Hohenpeissenberg ozonesondes (diamonds) and the FK climatology versus sondes (pluses). Here, c1 is the Pearson correlation for NNORSY, and c2 is for FK. Regression curves are printed dashed and dotted, respectively.

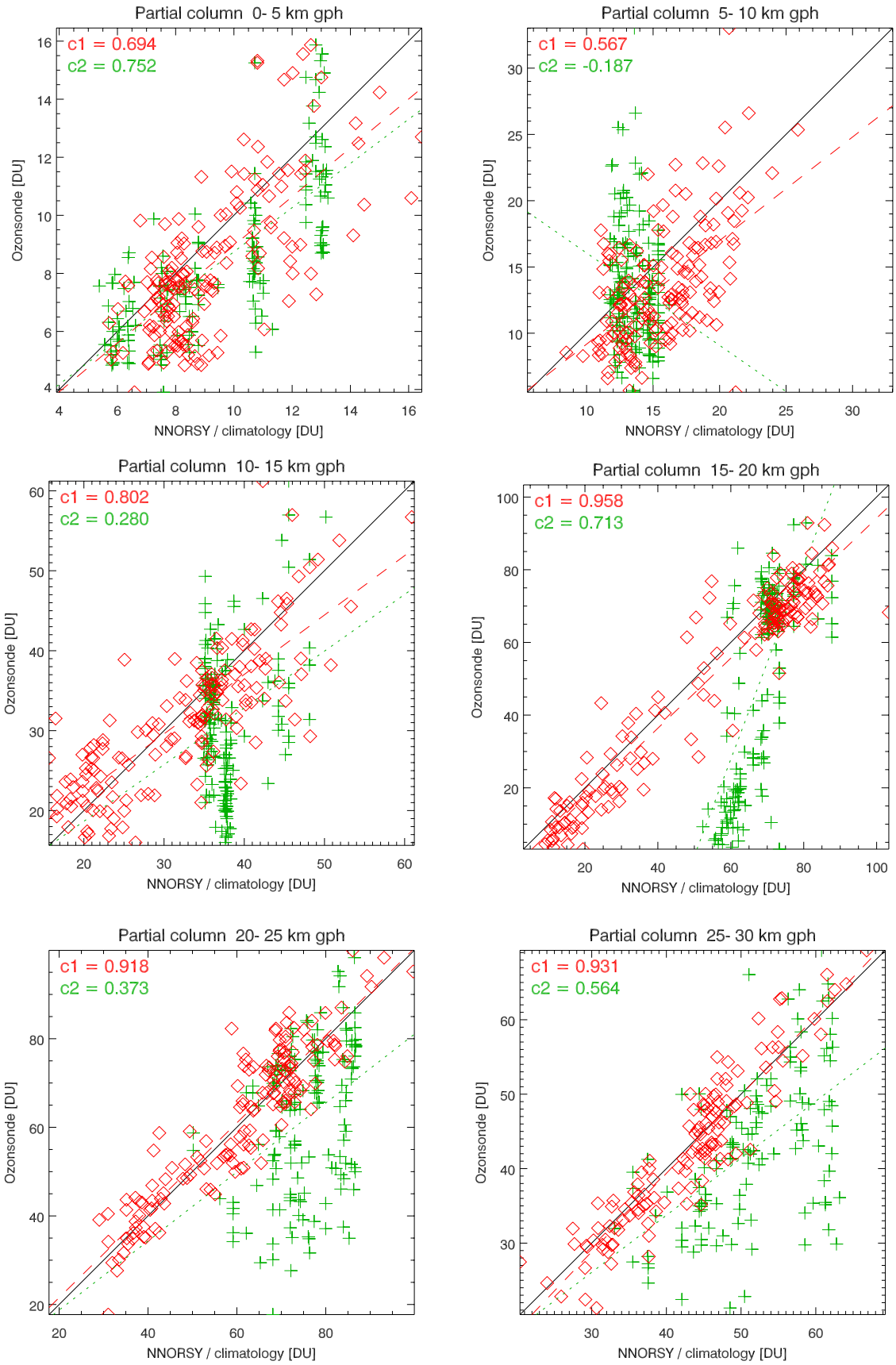

Figure 7. Same as Figure 6, but for station Syowa (69.0°S, 39.6°E).

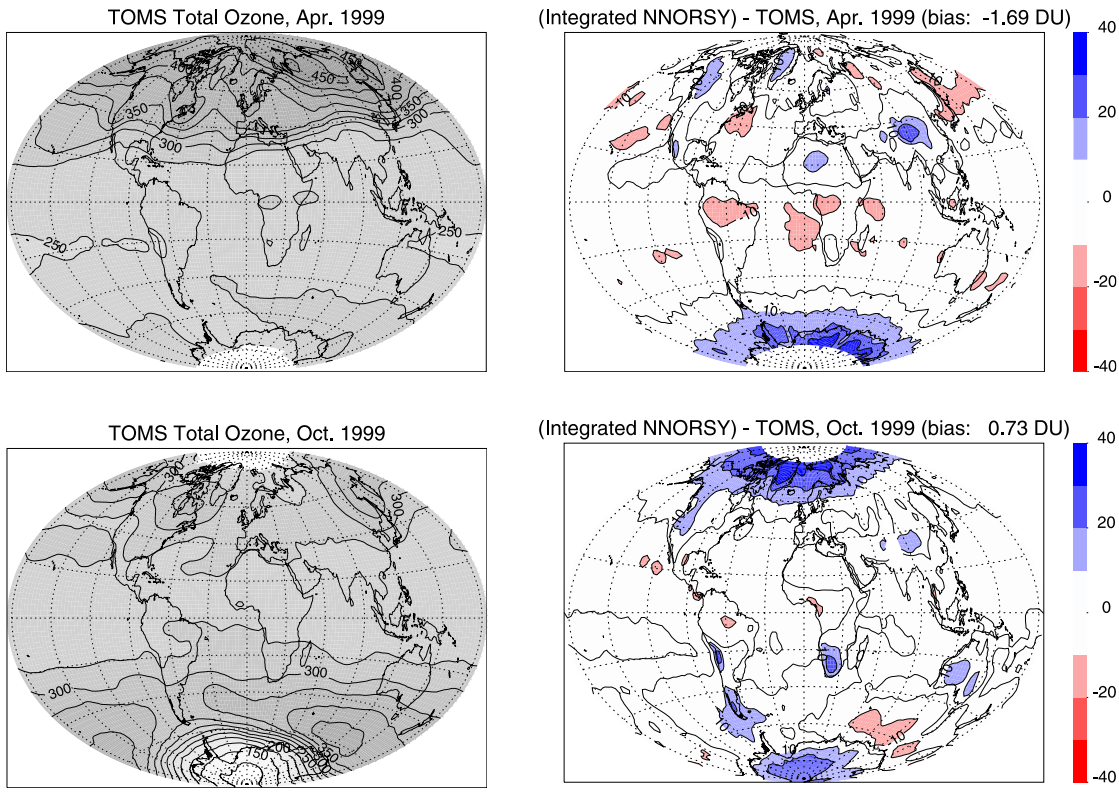

Figure 10. Monthly mean comparison of TOMS v7 total ozone with integrated NNORSY ozone profiles. All scales in DU.